BL Lacertae: Recovering intrinsic trajectory of a quasi-stationary jet feature on subparsec-scales

L.A. Hambardzumyan *[1,2], T.G. Arshakian †[1,3], and A.B. Pushkarev ‡[4]

[1]Byurakan Astrophysical Observatory after V.A. Ambartsumian, Armenia
[2]Astrophysical Research Laboratory of Physics Institute, Yerevan State University, Armenia
[3]I. Physikalisches Institut, Universität zu Köln, Zülpicher Strasse 77, Köln, Germany
[4]Crimean Astrophysical Observatory, Nauchny, Crimea

Abstract

Very Long Baseline Array (VLBA) observations allow us to investigate the fine structure and dynamics of the inner part of the BL Lacertae jet. Long-term VLBA monitoring at 15 GHz has revealed the existence of a quasi-stationary component (QSC) in the jet interior, located about 0.26 mas from the radio core, followed by superluminal moving radio components. The study of the QSC motion is important in order to shed light on the dynamics of the inner part of the relativistic jet on spatial scales of milliparsecs. The latter is problematic due to measurement errors on such scales. In addition, the apparent QSC motion is a combination of the intrinsic motion of the QSC and the radio core, which predominantly occurs in the direction of the jet axis. Careful error analyses and apparent trajectory smoothing techniques are important to reveal the QSC intrinsic motion. We use 164 epochs of VLBA monitoring of the jet in BL Lacertae, available as part of the MOJAVE program, to study the QSC motion. We apply a moving average method to filter out the core contribution, which allows the detection of QSC intrinsic motion and develop an algorithm to clean up the smoothed trajectory using QSC positioning errors. We find that the QSC intrinsic trajectory is a combination of irregular reversals occurring on scales from about 0.15 yr to 0.5 yr. An analysis of the estimates of the reversal characteristics is presented for smoothed and cleaned trajectories.

Keywords: *BL Lacertae objects: individual: BL Lacertae, galaxies: active, radio continuum: galaxies, galaxies: jets.*

1. Introduction

Blazars belonging to the class of radio-loud active galactic nuclei (AGN) are characterised by the presence of relativistic jets oriented at small angles with respect to the observer's line of sight. We focus on the study of the interior of the jet of the BL Lacertae object on sub-parsec scale using the Very Long Baseline Array (VLBA) observations. The observations on interferometric radio telescopes allow us to investigate the structure and dynamics of the jet on scales of milliarcseconds. Monitoring of BL Lacertae with the VLBA at 15 GHz has revealed a jet structure consisting of a bright radio core (apparent origin of the jet at which the optical depth of synchrotron radiation $\tau_\nu \approx 1$) and a quasi-stationary component (QSC) located at 0.26 mas and referred to as C7 and that moving superluminal components appear downstream the C7 component (Arshakian et al., 2020, Cohen et al., 2014, 2015). According to Cohen et al. (2015), the dynamics of the quasi-stationary C7 component has the potential to influence the outer jet behaviour, extending over distances of several hundred parsecs.

Using VLBA data of 116 observational epochs (1999–2016) available from the MOJAVE (Monitoring Of Jets in Active galactic nuclei with VLBA Experiments) program (Lister et al., 2018), Arshakian et al. (2020) showed that C7 exhibits predominantly superluminal velocities ($\sim 2c$) with an asymmetric brightness distribution on the sky both along and across the jet axis. They confirmed the connection between large C7 amplitudes of displacement vectors and the excitation of relativistic transverse waves during the active and

*hambardzumyanlian@gmail.com, Corresponding author
†t.arshakian@gmail.com
‡pushkarev.alexander@gmail.com

doi: https://doi.org/10.52526/25792776-23.70.2-328

stable phases of the jet. They found that the observed (apparent) C7 motion is a combination of the C7 proper motion and the core displacement, which typically occurs in the direction of the jet axis and due to resolution-dependent core bias and/or changes in particle density or magnetic field amplitude, and developed a method to estimate the statistical characteristics of the C7 intrinsic motion and the radio core motion. They showed that the contribution of both motions to the apparent motion of C7 is comparable. In order to perform a comprehensive analysis of the intrinsic trajectory of C7, we need to minimise the effect of the core displacement and treat carefully the C7 positioning errors. Here, we use data from 164 VLBA observations at 15 GHz within a period of 1999–2020 and apply a moving average filter to the apparent C7 trajectory to smooth out the core displacement effect and analyse the positional errors using a cleaning algorithm. The advantages and disadvantages of smoothing and cleaning the C7 trajectory and characteristics of C7 reversal motion are discussed.

BL Lacertae has a redshift $z = 0.0686$ (Vermeulen et al., 1995), which corresponds to a scale factor of 1.3 pc mas^{-1}, assuming $H_0 = 71$ km s^{-1} Mpc^{-1} , $\Omega_\lambda = 0.73$ and $\Omega_m = 0.27$ (Komatsu et al., 2009).

2. Observed trajectory of quasi-stationary component

Analysis of radio maps of VLBA observations over a 20-year period (1999–2020) revealed a radio core, a quasi-stationary component, and moving radio components (Lister et al., 2021). Figure 1 illustrates the separation of the radio components from the radio core with epoch. It is noticeable that the C7 component (marked in yellow) is 0.26 mas away from the radio core, and 37 components appear to emerge from C7. The slope of a linear fit of the moving components determines the apparent radial velocity. The components have a wide range of apparent speeds distributed between $3c$ and $10c$ expressed in units of the speed of light. Cohen et al. (2014) reported the highest apparent speed of $9.2c$ for moving features from 1996 to 2013. Similar maximum apparent speed $(10 \pm 1)c$ is estimated for the component number C52 (ejected in 2013.4) during the time period between 2013 and 2020.

Methods for data reduction, model construction and error estimation are given in Lister et al. (2009), Cohen et al. (2014, 2015) and Arshakian et al. (2020). To analyse the motion of C7, we use the displacement

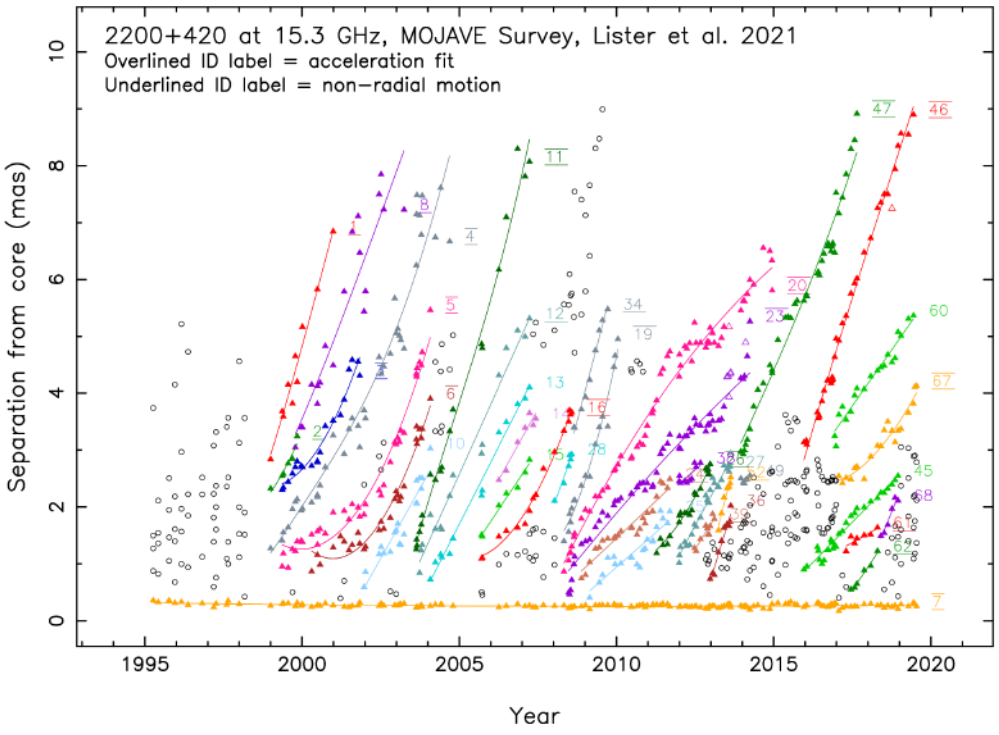

Figure 1: Separation of the components from the radio core[1]. Quasi-stationary C7 component (yellow triangles) is located at 0.26 mas from the core, moving components have superluminal speeds between $\approx (3 - 10)c$ (colored symbols).

[1]The plot is sourced from the MOJAVE web page.

doi: https://doi.org/10.52526/25792776-23.70.2-328

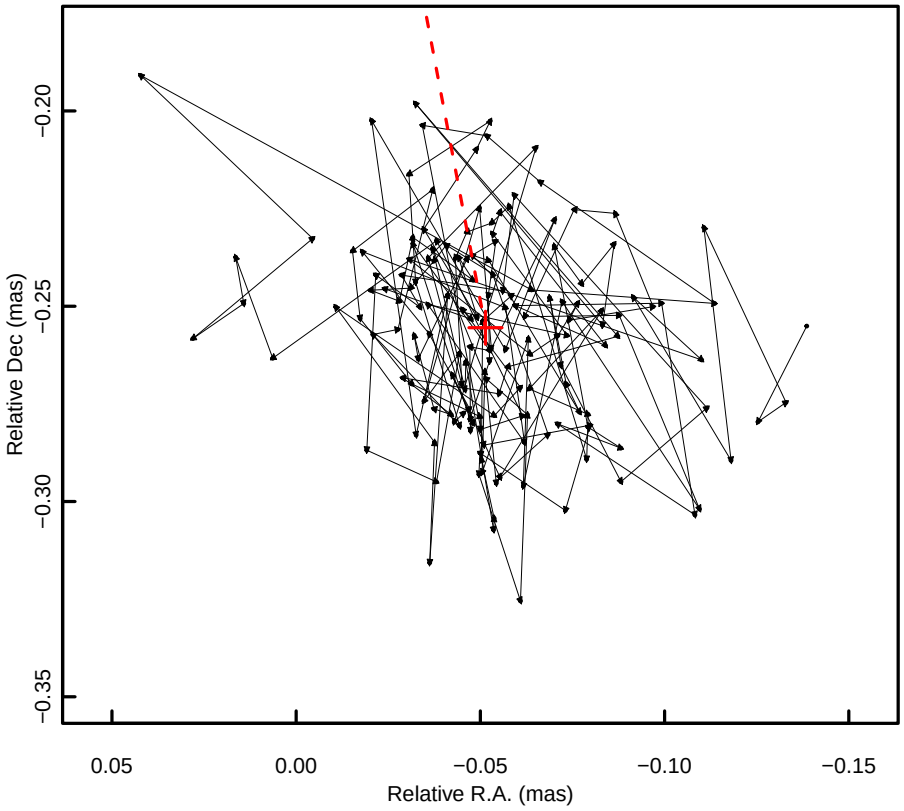

Figure 2: Observed trajectory of C7 in the RA–Dec plane. The central axis of the jet (red dashed line) connects the median position of C7 (red plus sign) and the radio core located at (0,0).

vector, which delineates the trajectory of C7 between two consecutive epochs of observations and indicates the direction of motion. The time intervals Δt between observations varied from a few days to several months with a median value of ≈ 30 days. The average C7 position uncertainties along and across the jet were estimated by Arshakian et al. (2020) to be 5 μas and 2 μas, respectively. They considered these values as lower limits, while real errors can exceed these estimates by a factor of 1.5–2.

Figure 2 shows the observed trajectory of C7 for a time period 1999.37–2019.97. The median center is at position $\mathrm{RA_{med}} = -0.051$ mas and $\mathrm{Dec_{med}} = -0.255$ mas. The dashed line connecting the radio core and the median center of C7 is the central axis of the jet, at the positional angle $\mathrm{PA} = -169°$. The observed trajectory of C7 appears complex and zigzagging mainly due to significant displacements of the radio core along the jet axis.

3. Smoothing and cleaning the trajectory of C7

As we discussed above, to recover the C7 intrinsic motion it is essential to smooth out the wobbling of the core which happens primarily along the jet direction. For this we apply the moving average filter with a sliding window of four positions to smooth the observed trajectory on scales of ~ 0.05 mas. The size of the sliding window seems to be optimal for preserving the C7 intrinsic trajectory (Hambardzumyan et al., 2023), which is shown in Figure 3. Certain structural patterns such as oscillatory and reverse motions on various spatial scales are visible. Visual inspection of the smoothed trajectory is described in Hambardzumyan et al. (2023).

In addition to the core displacements, the observed C7 trajectory is affected by large positional uncertainties. Asymmetric 1σ positional errors of the C7 location overlap when the displacement is relatively small (Figure 4, left panel). This can lead to unreliable measurements of displacement vectors. To eliminate such non-robust displacements we propose a trajectory refinement algorithm. The algorithm works as follows: the length of the displacement vector (r) between two consecutive positions, and the positioning errors along the displacement vector (σ_1 and σ_2) are calculated. If r is greater than or equal to $\sigma_1 + \sigma_2$ (the ellipses do not intersect), the two positions are considered distinct; if r is less than $\sigma_1 + \sigma_2$ (the ellipses intersect), the algorithm discards the position with the larger error. This iterative process is applied to each pair of

doi: https://doi.org/10.52526/25792776-23.70.2-328

positions. The resulting refined trajectory is shown in Figure 4 (right panel) for the time period between 1999 and 2005. A detailed look at Figure 4 shows that some trajectory patterns have undergone changes after the refinement of the smoothed trajectory. In the left panel of Figure 4, the loop-like pattern positioned at about $(-0.07, -0.24)$ and having the counterclockwise motion turned into a clockwise sharp reversal (right panel). Transformation occurs also for the loop-like motions located at around $(-0.058, -0.277)$ and $(-0.047, -0.24)$ (see Figure 4, left panel). A total of five loop-like structures and seven reversed trajectories with a spatial scale of less than 0.01 mas (corresponding to a time scale of about 0.45 yr) transformed or flattened during the 20-year time period after the refinement procedure. Three of these trajectories changed their direction from anti-clockwise to clockwise. The full refined C7 trajectory for the time period from 1999 to 2020 is shown in Figure 5.

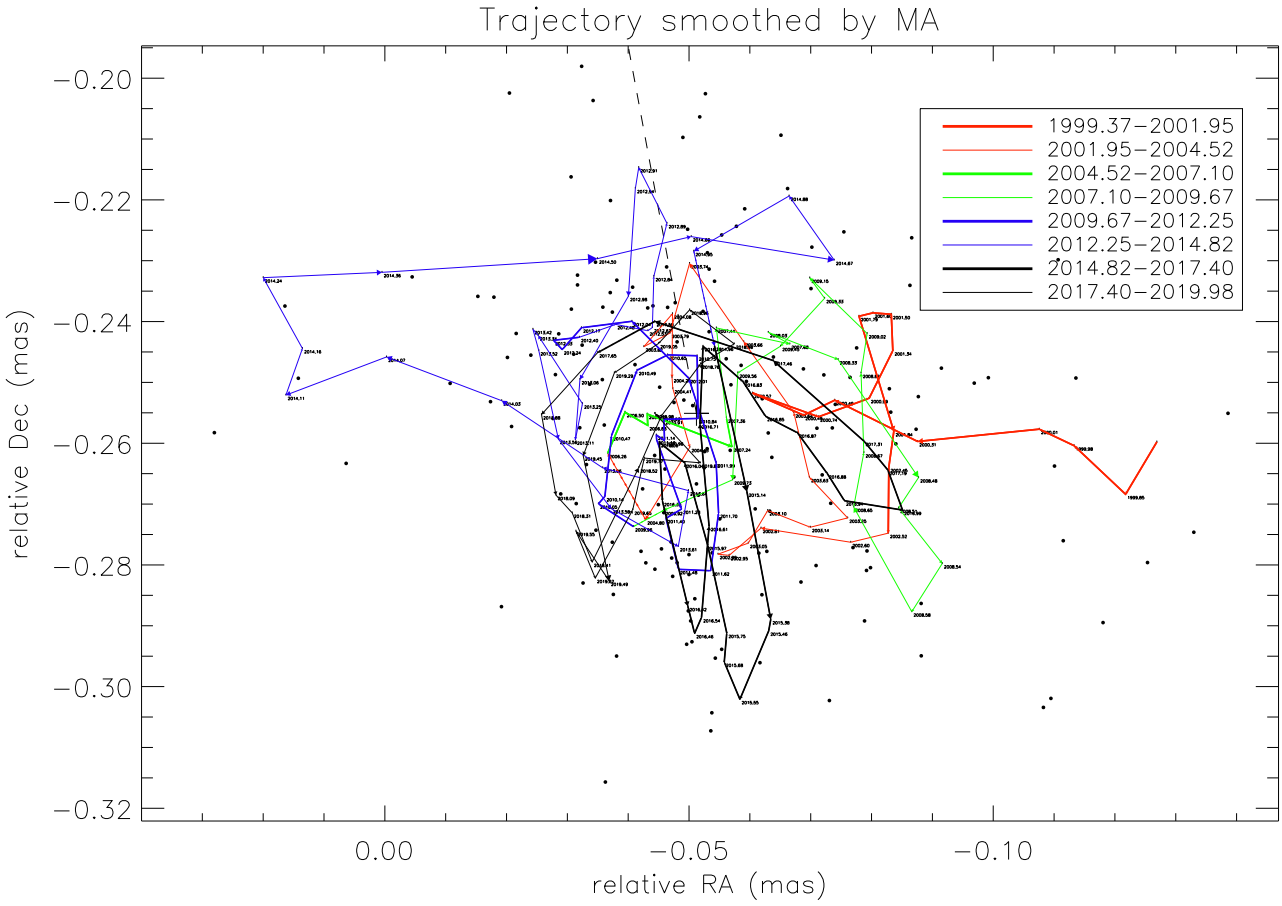

Figure 3: The apparent trajectory of C7 smoothed by moving average method with a sliding window of length $m = 4$. The numbers along the smoothed trajectory are the observation epochs in years (yr). The observed positions of C7 component are marked by dots. The radio core is at $(0, 0)$ position, which is connected with the median position of C7 (plus sign) by the jet central axis (dashed line). Thick and thin colored lines represent the time intervals of 2.95 yr. Arrows indicate the direction of movement.

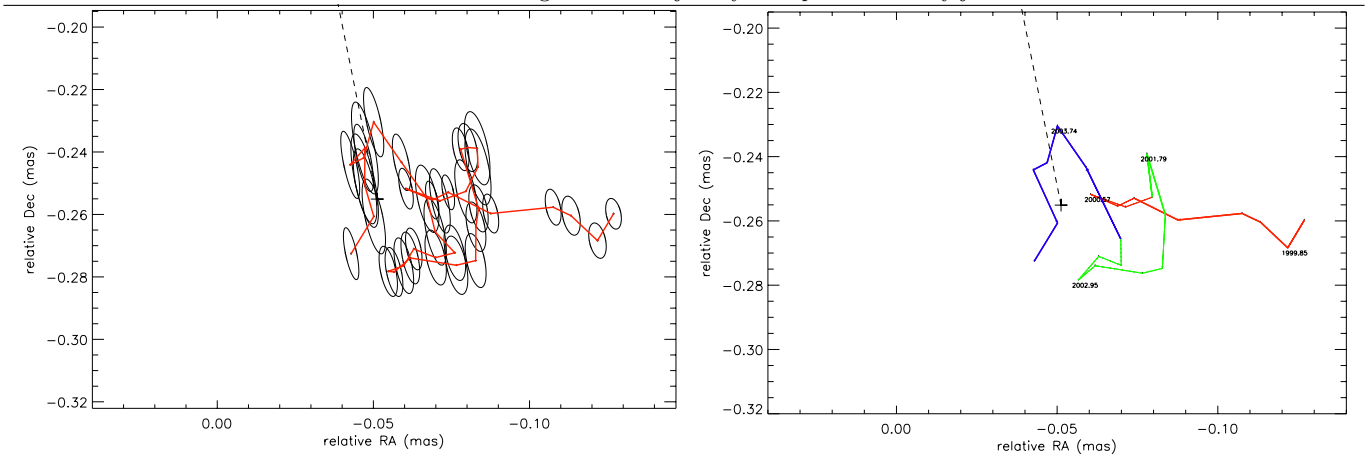

Figure 4: The smoothed C7 trajectory (left panel) and its refined version (right panel) are shown for the time interval 1999-2005. In the left panel, the asymmetric positioning errors are represented as ellipses where large and small radii correspond to the positioning errors along and across the jet axis, respectively. In the right panel, the turning points of the reversals are labelled by the epoch of observations.

Approximately 27% of positions are discarded by the cleaning algorithm, effectively eliminating trajectories on spatial scales $\lesssim 0.01$ mas (or 0.013 pc). The refined trajectory is further used for detailed investigation and classification. Upon visual examination of the trajectory, we observe both quasi-regular and irregular reverse motions. Reversible trajectories are either straight or curved and are accompanied by the occurrence of arc-shaped, loop-shaped, and W-shaped configurations as a turning point, although the latter are less common. The quasi-regular motion of C7 has a characteristic period of about 1.4 yr.

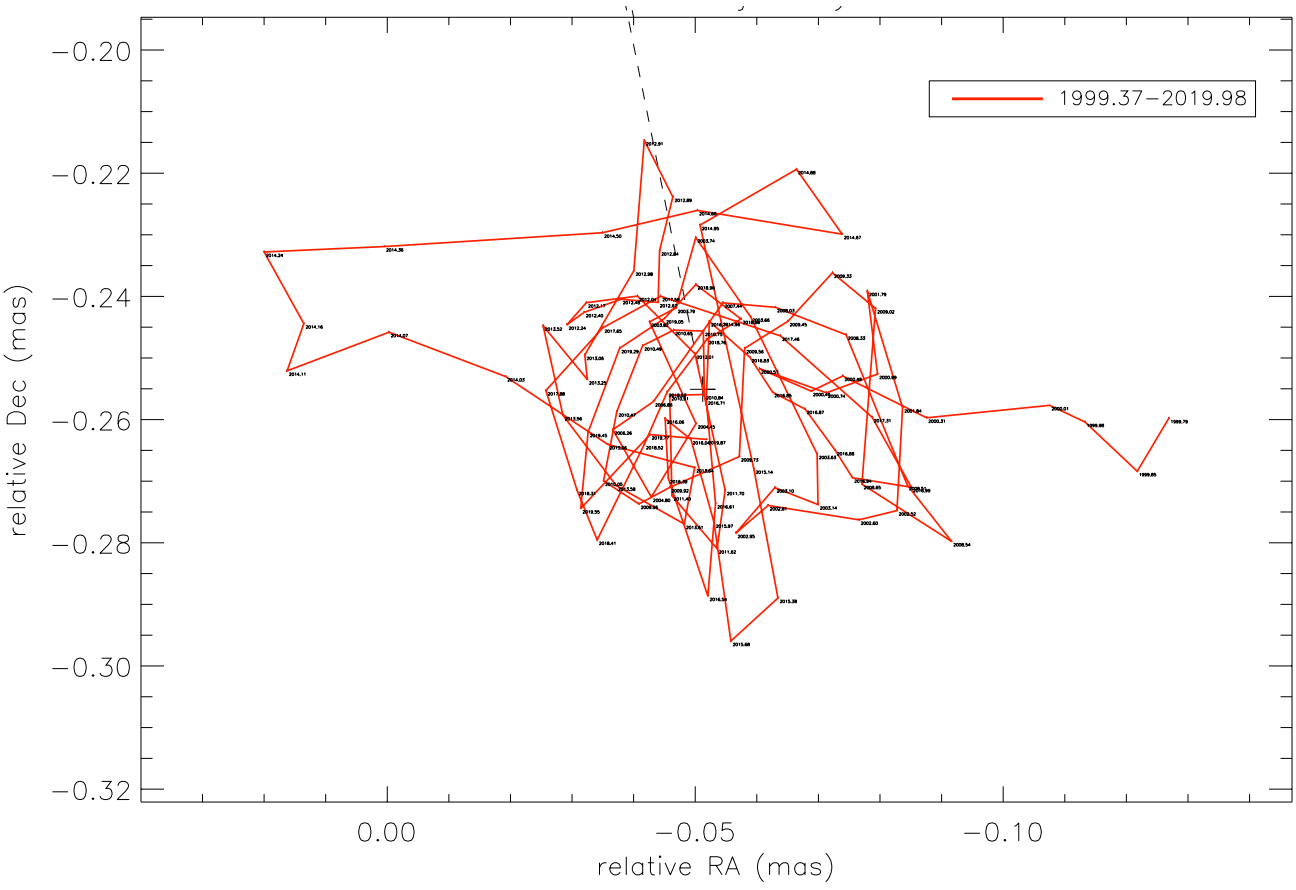

Figure 5: Refined trajectory of the smoothed C7 apparent trajectory. The radio core is at $(0, 0)$ position, which is connected with the median position of C7 (plus sign) by the jet central axis (dashed line). The numbers along the trajectory are the epochs of observations in years from which the direction of motion can be determined.

4. Characteristics of reversals

The refinement procedure eliminates scales smaller than 0.01 mas and improves the reliability of displacement vector measurements. The latter allows us to define a reversal as a trajectory in which two consecutive displacement vectors have an angle less than 90° at the turning point. A total of 24 reversals are identified, which are further classified as U-turns (angles $< 45°$), V-turns (angles $> 45°$ and $< 90°$), and loop-like reversals. The distribution of 22 distances between turning points of the reversals is shown in the Figure 6 (the distance between 2004.8 and 2006.4 is excluded from the calculations because of the large gap between observations). The distribution is not uniform, it appears to have two peaks at ~ 0.05 mas and ~ 0.11 mas. The mean value of the distances between turning points is 0.062 mas, and the standard deviation is 0.029 mas.

We now compare the reversal characteristics of the smoothed trajectory (Hambardzumyan et al., 2023) and the refined trajectory. We measure these characteristics in the same way as described in Hambardzumyan et al. (2023). After trajectory refinement, the time intervals between successive reversals typically range from 0.1 yr to 1.4 yr, excluding the two outliers. The typical reversal period is about 0.65 ± 0.08 yr. Prior to trajectory refinement, the median time interval is 0.50 ± 0.09 yr. The azimuthal angle, which is the angle between the jet axis and the line connecting the median centre and the turning point, has a uniform distribution for both smoothed and refined trajectory reversals. The distributions of radial distances from the median centre of the scattered positions to the turning points of the reversals have clustering around 0.029 ± 0.003 mas and 0.032 ± 0.004 mas for the smoothed and refined trajectories, respectively. In general, the estimates of the statistical characteristics of the reversals for these two trajectories coincide within the errors.

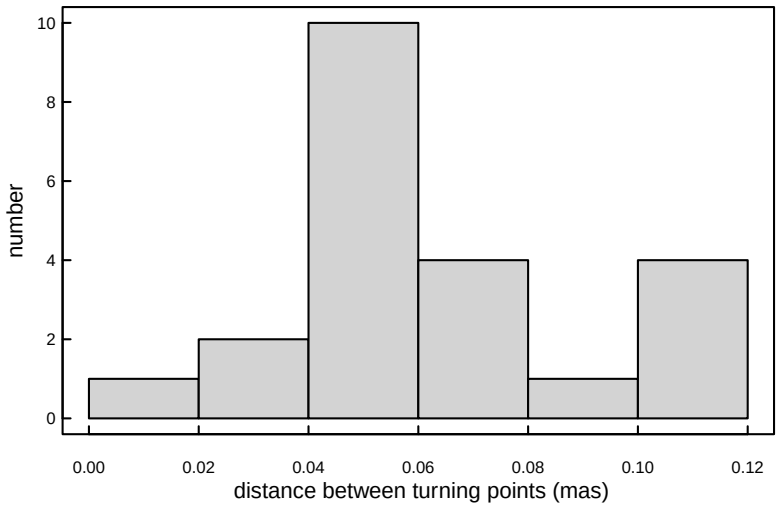

Figure 6: The distribution of distances between turning points of 22 reversals.

Acknowledgements

The VLBA is a facility of the National Radio Astronomy Observatory, a facility of the National Science Foundation that is operated under cooperative agreement with Associated Universities, Inc. This research has made use of data from the MOJAVE database that is maintained by the MOJAVE team (Lister et al., 2018).

References

Arshakian T. G., Pushkarev A. B., Lister M. L., Savolainen T., 2020, Astron. Astrophys. , 640, A62

Cohen M. H., et al., 2014, Astrophys. J. , 787, 151

Cohen M. H., et al., 2015, Astrophys. J. , 803, 3

Hambardzumyan L. A., Arshakian T. G., Pushkarev A. B., 2023, Communications of the Byurakan Astrophysical Observatory, 70, 94

Komatsu E., et al., 2009, Astrophys. J. Suppl. Ser. , 180, 330

Lister M. L., et al., 2009, Astron. J. , 138, 1874

Lister M. L., Aller M. F., Aller H. D., Hodge M. A., Homan D. C., Kovalev Y. Y., Pushkarev A. B., Savolainen T., 2018, Astrophys. J. Suppl. Ser. , 234, 12

Lister M. L., Homan D. C., Kellermann K. I., Kovalev Y. Y., Pushkarev A. B., Ros E., Savolainen T., 2021, Astrophys. J. , 923, 30

Vermeulen R. C., Ogle P. M., Tran H. D., Browne I. W. A., Cohen M. H., Readhead A. C. S., Taylor G. B., Goodrich R. W., 1995, Astrophys. J. Lett. , 452, L5